Journal of Innovative Optical Health Sciences
Vol. 2, No. 1 (2009) 45–60

World Scientific
www.worldscientific.com

MULTIPHOTON MICROSCOPY: A NEW APPROACH IN PHYSIOLOGICAL STUDIES AND PATHOLOGICAL DIAGNOSIS FOR OPHTHALMOLOGY

CHIU-MEI HSUEH[*], WEN LO[*], SUNG-JAN LIN[‡,§], TSUNG-JEN WANG[¶], FUNG-RUNG HU[‖], HSIN-YUAN TAN[**,††] and CHEN-YUAN DONG[*,†]

[*]*Department of Physics*
National Taiwan University
Taipei 106, Taiwan, China
[†]*cydong@phys.ntu.edu.tw*

[‡]*Institute of Biomedical Engineering*
National Taiwan University Taipei
106, Taiwan, China

[§]*Department of Dermatology*
National Taiwan University Hospital
Taipei 100, Taiwan, China

[¶]*Department of Ophthalmology*
Taipei Medical University
Hospital Taipei 100, Taiwan, China

[‖]*Department of Ophthalmology*
National Taiwan University, College of Medicine and Hospital
Taipei 100, Taiwan, China
fungrong@ntu.edu.tw

[**]*Department of Ophthalmology*
Chang-Gung University
Linko 333, Taiwan, China

[††]*Institute of Biomedical Engineering*
National Taiwan University
Taipei 100, Taiwan, China
d93548010@ntu.edu.tw

Multiphoton microscopy (MPM), with the advantages of improved penetration depth, decreased photo-damage, and optical sectioning capability, has become an indispensable tool for biomedical imaging. The combination of multiphoton fluorescence (MF) and second-harmonic generation (SHG) microscopy is particularly effective in imaging tissue structures of the ocular surface.

[†,‖,††]Corresponding authors.

This work is intended to be a review of advances that MPM has made in ophthalmic imaging. The MPM not only can be used for the label-free imaging of ocular structures, it can also be applied for investigating the morphological alterations in corneal pathologies, such as keratoconus, infected keratitis, and corneal scar. Furthermore, the corneal wound healing process after refractive surgical procedures such as conductive keratoplasty (CK) can also be studied with MPM. Finally, qualitative and quantitative SHG microscopy is effective for characterizing corneal thermal denaturation. With additional development, multiphoton imaging has the potential to be developed into an effective imaging technique for *in vivo* studies and clinical diagnosis in ophthalmology.

Keywords: Multiphoton microscopy; fluorescence; second harmonic generation; cornea; sclera.

1. Introduction

1.1. *Normal cornea structure*

The eye is a highly specialized organ of photoreception and is composed of numerous functional units working in unison. On the frontal surface, the transparent cornea is responsible for more than two-thirds of the eye's focusing power. Immediately adjacent to the cornea is the opaque sclera which forms the remaining five-sixth of the outer coating of the eye and is largely responsible for structural integrity and protection of the intraocular contents. At the boundary between the cornea and the sclera lies the limbus, which contains stem cells responsible for maintaining the corneal epithelium. Like the cornea, the sclera is primary composed of collagen fibers and is covered by epithelial conjunctiva.

Among the different structures of the ocular surface, the important role of cornea in visual function is of intense interest to researchers. From light and electron microscopy, it is known that the cornea consist of the following layers: epithelium, Bowman's membrane, stroma, Descemet's membrane, and the endothelium. At the anterior side, the corneal epithelium is made of a thin multilayer (five to six layers) of squamous, nonkeratinized epithelial cells. Below the epithelium lies the Bowman's layer which is an acellular region consisting of densely and randomly arranged thin collagen fibrils (types I, III, V, and VI) that separate the epithelium from the stroma. The stroma which makes up 90% of the cornea is a layered structure consisted of stacked lamellae. Each lamella is composed primarily of regularly arranged type I collagen fibrils, with keratocytes distributed within the lamellar layers. The Desemet's membrane is a thin, acellular, and homogeneous layer adjacent to the posterior stroma and the endothelium. Finally, the corneal endothelium is a mono-layer of simple squamous tissue located at the posterior surface of the cornea.[1–5]

Traditionally, ophthalmology has depended heavily on traditional histological procedures for morphological studies. However, histological examination and electron microscopy involve the process of fixation and staining that can result in artifacts in the obtained structural information. Furthermore, the high transparency of cornea increases the difficulty of observing corneal structure by conventional optical microscopy. Over the last few decades, new imaging techniques that overcome limitations of the histological approach, such as slit lamp microscopy, optical coherence tomography (OCT), reflective confocal microscopy, and multiphoton microscopy (MPM), have been developed for furthering our understanding of corneal physiology and pathology.

1.2. *Slit lamp*

The slit lamp is an instrument consisting of a high-intensity light source from a lamp source that can be focused through the slit for specimen illumination. A long working distance objective is used for focusing and achieving magnified three-dimensional (3D) imaging.[1] This technique was developed approximately 100 years ago and is used for the examination of the corneal endothelium.[2,3] Clinically, it can also be used to observe the cornea, the ocular lens, and the retina[4,5] and a variety of ophthalmologic pathologies can be diagnosed.[6]

1.3. *Optical coherence tomography*

Optical coherence tomography (OCT), an imaging technique that depends on the interference

from the layers within biological tissues, has been used in a variety of medical applications, including those in ophthalmology.[6–9] The OCT provides cross-sectional imaging with micron resolution,[10] and can correctly reveal corneal morphology despite its high transparency. Furthermore, since the axial resolution depends on the coherence length rather than the numerical aperture (NA), OCT can clearly visualize layered structure from the anterior to the posterior segment of the eye.[9,11,12] The application of OCT on the human cornea was first reported in 1994,[12] which mapped contours of the epithelium and endothelium, and quantitatively analyzed the corneal thickness. Hoerauf *et al.*[13] utilized slit-lamp-adapted OCT to investigate the corneal morphology before and after phototherapeutic keratectomy, and demonstrated the potential of the technique as a medical diagnostic tool. Recently, OCT has also been used to characterize the corneal pathologies, such as bullous keratopathy,[6] corneal edema,[14] and macular disease.[15] New development of this technique includes combining OCT with improved broad-bandwidth for improving resolution in biomedical applications.[7]

1.4. *Reflective confocal microscopy*

Confocal microscopy is a high-resolution optical imaging technique first invented by Marvin Minsky in 1957.[16] It is depth-resolved by utilizing a pinhole to allow detection of emissions only from the focus of the excitation light source. Reflective confocal microscopy combines the principle of confocal microscopy with the contrast mechanism provided by the reflection that occurs at the interface between materials with different refractive indices. This minimally-invasive method has been applied clinically and used in ophthalmologic investigation. A real-time direct view confocal microscope based on a spinning Nipkow disk[17] was first utilized to show nerve fibers morphology within thin optical sections of an *ex vivo* animal cornea.[18] Subsequently, *in vivo* and *ex vitro* cornea images obtained using confocal microscopy with advanced instruments clearly revealed epithelial and endothelial cells, and the various shapes of stromal keratocytes.[19–21] Reflective confocal microscopy was also used to observe the wound healing after refractive surgeries,[22–29] helped to determine the possible causes of complications arising from surgeries. Recently, reflective confocal microscopy has also been applied for *in vivo* ophthalmologic observation[30–32] and for the detection of corneal diseases such as infectious keratitis and keratoconus.[33–38]

2. Multiphoton Microscopy (MPM)

2.1. *Potential of multiphoton imaging in ophthalmology*

In recent years, another imaging technique that has become an indispensable tool for biomedical imaging is multiphoton fluorescence (MF) microscopy pioneered by Webb's group.[39] In MF imaging, near-infrared photons are used for non-linear fluorescence excitation of the specimens. This approach has optical sectioning capability as confocal microscopy, but with additional advantages of an improved penetration depth, more effective light collection, and decreased photo-damage.[39–41] In addition, MPM can also be used to induce second harmonic generation (SHG) from biological tissues with non-centrosymmetric structures and can provide complementary structural information of the cornea to other techniques such as slit lamp, OCT, and confocal microscopy. The major difficulty with corneal imaging is its optical clarity which hinders the direct observation of cornea structure using standard optical microscopy. However, using MPM, NAD(P)H autofluorescence (AF) can be used to monitor the cell metabolic activities.[42,43] Moreover, label-free imaging of corneal or sclera collagen fibrils can only be achieved by detecting the SHG signal.[44,45]

2.2. *Basic principles of multiphoton excitation*

The principles of two-photon excitation were theoretically predicted by Maria Göppert-Mayer in 1931.[46] However, direct experimental confirmation was not achieved until 1961 by Kaiser and Garrett.[47] The incorporation of two-photon fluorescence into a laser scanning microscope system was first demonstrated in 1990.[39] In addition, the discovery of non-linear optical effect such as SHG[48] led to the realization of microscopic imaging in the 1970s.[49]

The MPM is capable of providing 3D imaging capability using the non-linear excitation of fluorophores. The optical sectioning capability is associated with the excitation process. Specifically, non-linear excitation occurs from the near-simultaneous absorption of two or more photons.

The probability of simultaneous two-photon absorption can be determined quantum mechanically and the results show that two-photon excited signal depends on the square of incident photon flux. In order to generate the instantaneously high-photon flux necessary for an efficient multiphoton excitation, a focusing objective is usually used to spatially confine an ultrafast excitation source. In this manner, most of two-photon generated fluorescence occurs at the focal region. The localized excitation volume not only improves the axial depth discrimination and image contrast but also reduces out-of-focus photo-damage compared to one-photon excitation. Moreover, the near-infrared light photons used in MPM are absorbed and scattered less by tissue components, thus allowing greater imaging depths to be achieved.[39,40,50,51] The distinct features of two-photon microscopy allow observation of living specimens without detectable damage as it is as an effective biological imaging tool *in vivo*.

2.3. *Second harmonic generation SHG microscopy*

Harmonic generation is a non-linear polarization process related to the interaction of intense light with matters. In general, the polarization, P, of a material can be expressed as:

$$P = \chi^{(1)}E + \chi^{(2)}E^2 + \chi^{(3)}E^3 + \cdots, \qquad (1)$$

where $\chi^{(1)}$, $\chi^{(2)}$, and $\chi^{(3)}$ are, respectively, the first-, second-, and third-order susceptibility tensors, and E is the applied electric field. The second term $\chi^{(2)}E^2$ represents the induced SHG polarization, which contributes to radiation at twice the frequency of the incident excitation source. Accordingly, the SHG intensity depends on the square of the incident light intensity in a manner similar to the two-photon-induced-fluorescence process. As a result, imaging with the SHG signal produces images with superior axial depth-discrimination with intrinsic sectioning capability.[49] Moreover, since the energy of the SHG photon is equivalent to the combined energy of two photons of the excitation source, therefore, energy is not deposited on the illuminated specimen. This feature allows microscopic imaging to be achieved with minimal invasion.[52] In ophthalmologic applications, collagen is known as the predominant constituent of corneal stroma[53] and as a SHG generator due to the intrinsic triplehelix, non-centrosymmetric, structure.[54] Therefore, the second harmonic generating structure of collagen could lead to imaging of corneal stroma without extra labels.[55–58]

2.4. *Multiphoton microscopy (MPM) instrumentation*

A typical multiphoton imaging system is shown in Fig. 1. For excitation, a titanium-sapphire (ti-sa) laser (Tsunami, Spectra Physics, Mountain View, California) pumped by a diode-pumped, solid-state (DPSS) laser system (Millennia X, Spectra Physics) is used. The 780-nm output of the ti-sa laser is used for sample excitation and can be guided into a commercial upright microscope (E800, Nikon, Japan)

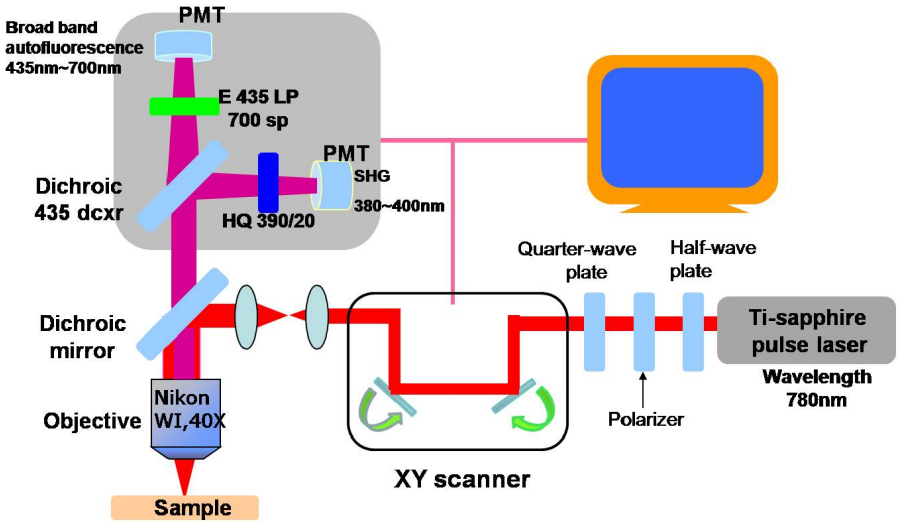

Fig. 1. The experimental set-up of a custom-built multiphoton microscope.

by a pair of galvanometer-driven, x–y mirrors (Model 6220, Cambridge Technology, Cambridge, Massachusetts). After entering the microscope, the laser light is beam-expanded and reflected by the short-pass, primary dichroic mirror (700 dcspruv-3p, Chroma Technology, Rockingham, Vermont) onto the back aperture of the focusing objective (such as S Flour, 40X, NA 0.8, WI, Nikon). Multiphoton images can then be acquired by scanning the focused spot that is scanned across the specimen. In order to obtain 3D images at both high-resolution and large-scale, a motorized stage (H101, Prior Scientific, United Kingdom) is adapted to the microscope for specimen translation after each optical scan. The emitted signals are collected by the focusing objective in the epi-illuminated geometry. First, the signals pass through the primary dichroic mirror, the broadband multiphoton autofluorescence (MAF) and SHG signals are then separated by a secondary dichroic mirror (435dcxr, Chroma Technology) and respectively filtered by two band-pass filters (MAF: E435lp-700sp, SHG: HQ390/20, Chroma Technology) before reaching the detectors. For signal detection, photon-counting photomultiplier tubes (R7400P, Hamamatsu, Japan) can be used. The detection bandwidths of the broadband fluorescence and SHG bandwidths used in our laboratory are 435–700 nm and 380–400 nm, respectively.

3. Applications of MPM in Ophthalmic Imaging

3.1. *Corneal morphology revealed by MPM*

The distinct advantages of MPM enable this technique to be widely applied in many areas of biomedical researches including ophthalmology. Specifically, the ability to acquire structural information is of key significance in the physiological studies and the disease diagnosis of the eye. In previous reports, multiphoton and SHG microscopy has been used to investigate the cellular structure and collagen orientation within the cornea.[43,57,59] Specifically, it was shown that AF of epithelium and endothelium cells is from NAD(P)H.[43] In a later work, backward SHG microscopy was used to reveal the 3D collagen organization within the corneal stroma.[57] Furthermore, SHG microscopy was also used to characterize the different orientations of collagen within the cornea and sclera.[59]

In addition to localized imaging of the ocular surface, MPM also can be used to map the ocular structure on a large geometric scale.[60] As shown in Figs. 2–4, MAF and SHG microscopy is an effective technique for obtaining spectrally-resolved morphological features of the cornea, limbus, conjunctiva, and sclera in whole, *ex vivo* normal porcine eyes. In Fig. 2, large-area multiphoton scans on the porcine corneal surface at the depth of 0 μm and 862 μm are shown. In addition, magnified views of selected regions of interest (I and II) are shown in Figs. 2(c) and (d), respectively. At the corneal surface (0 μm), individual cells can be identified by the AF cytoplasm and dark nuclei. The cellular morphology of the corneal epithelium revealed by AF signal is consistent with the characteristics of the epithelial cell mentioned previously. Furthermore, SHG signal from the collagen fibers is also visible at the corneal surface because the structurally intact porcine eye preserves the natural curvature of the cornea. At the depth of 862 μm from the corneal surface, emitted AF can be used to image the innermost layer of the cornea. In addition, collagen organization can be visualized by SHG microscopy. Another important component of the ocular surface, the limbus, can also be effectively imaged by AF imaging and the results at the depths of 0 and 50 μm are shown in Fig. 3. Similar to the imaging results of the corneal epithelium, limbal cells can be identified by AF cytoplasm and non-AF nuclei. In addition, the corneal and scleral collagen can be visualized by SHG signal. At the depth of 50 μm, it was observed that the width of the limbus epithelial tissues decreases while the cornea and sclera collagen start to merge. This observation is consistent with the known morphological features of the limbus. In addition to imaging cornea and limbus, MPM can be used to reveal morphological information of the conjunctiva and the sclera (Fig. 4). However, the achievable imaging depths using SHG signal for visualization of sclera collagen is less compared to the optically transparent cornea. In addition, note that imaging the keratocytes inside the stroma with AF is more difficult due to their slow metabolism that leads to a decrease in the amount of NAD(P)H. This is due to the fact that since the redox reaction of NAD(P)H can influence the fluorescence yield, AF intensity may be used as an indicator of cellular respiration and therefore as an intrinsic probe of cellular metabolism. In the case of corneal wound healing, keratocytes whose AF could

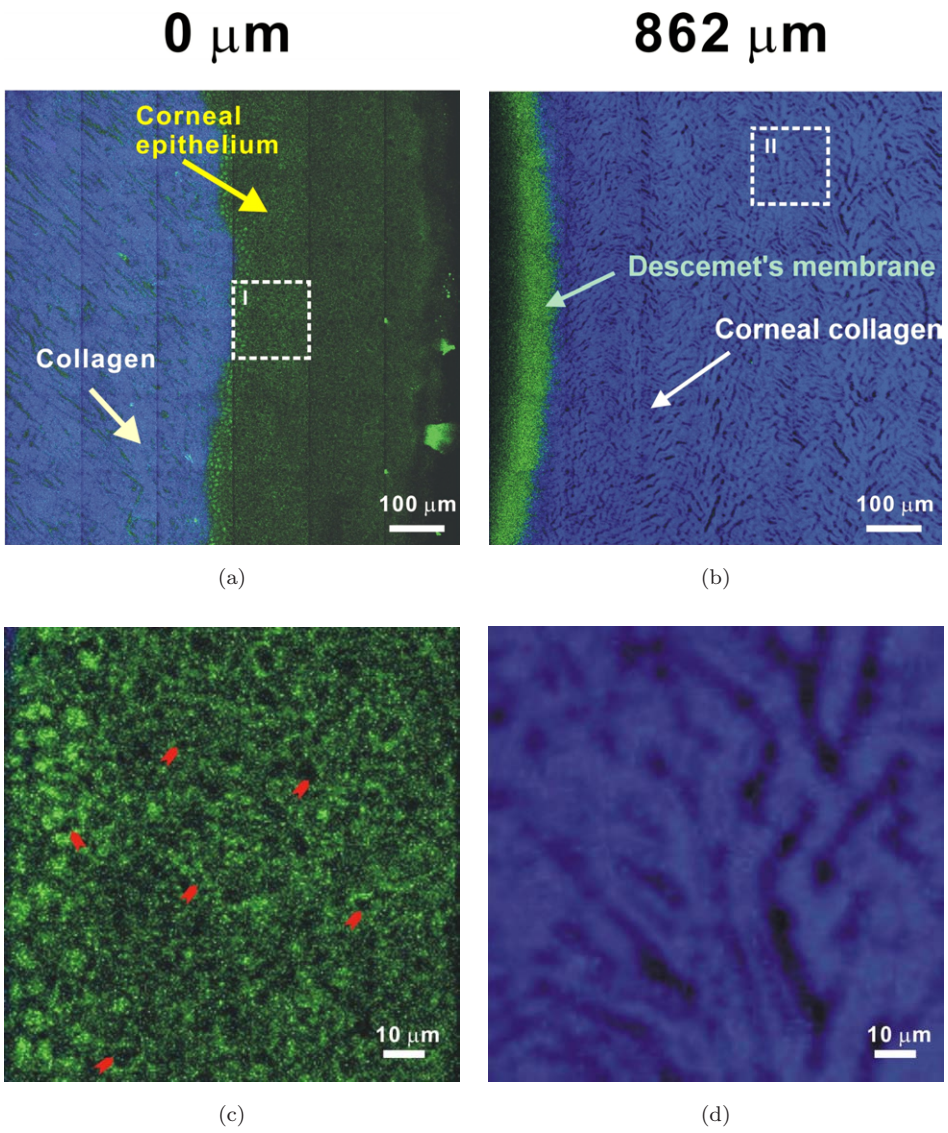

Fig. 2. (a) Large-area multiphoton images at the surface (0 μm) of porcine cornea; (b) Large-area multiphoton images at the bottom (862 μm); (c) The magnified image of selected area I in (a) displays the AF cytoplasm (green) and dark nuclei (arrowheads) of epithelium, and (d) The magnified collagen image of selected area II in (b) is shown. (*Blue*: SHG; *green*: autofluorescence). Reproduced with permission.

not be seen under normal respiration can become apparent during corneal wound healing.[43]

In addition to obtaining regional information of the corneal architecture, structural map across the whole cornea can also be achieved using MPM. Using a transgenic green fluorescent protein (GFP) mouse (FVB-Tg-eGFP), GFP-tagged keratocytes can be visualized using MPM imaging. Moreover, the magnified images of Fig. 5(a) show that the keratocytes (Fig. 5(b)) and the epithelium (Fig. 5(c)) can be imaged by the fluorescence signals. In addition, the global organization of stromal collagen can be characterized (dashed lines in Fig. 5(a). Specifically, one can easily take notice of the fact that the corneal collagen is organized in concentric patterns.[61] Since the reason of the supra-structural organization of corneal collagen is not understood, the large-area multiphoton imaging approach may be used to probe the structure-function relationship of biological tissues.[62]

3.2. *Pathological corneal morphology revealed by MPM*

3.2.1. *Collagen reorganization in keratoconus*

Keratoconus is a non-inflammatory corneal disorder characterized by progressive corneal steepening and stromal thinning.[63] Clinically, this disease may

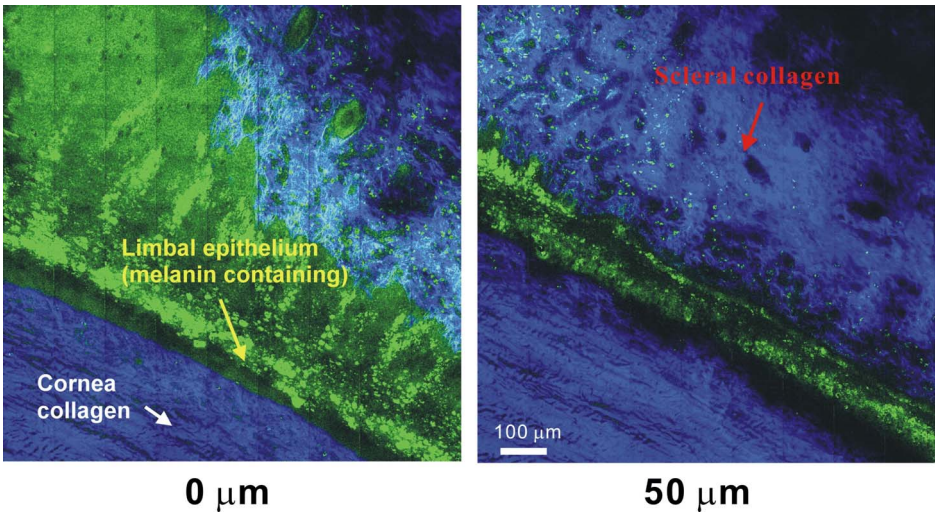

Fig. 3. Large-area multiphoton images of a porcine limbus at depths of 0 and 50 μm. (*Blue*: SHG; *green*: autofluorescence). Reproduced with permission.

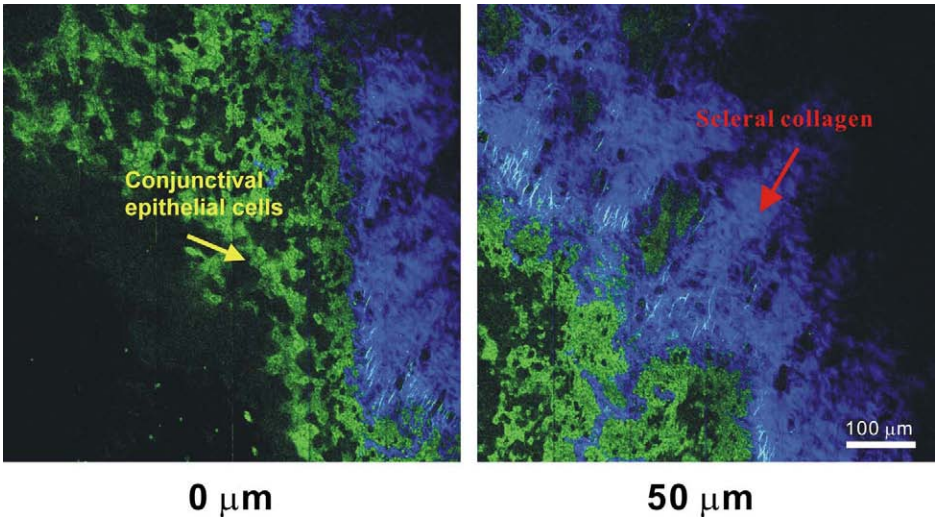

Fig. 4. Large-area multiphoton images of porcine conjunctiva and sclera at depths of 0 and 50 μm. (*Blue*: SHG; *green*: autofluorescence). Reproduced with permission.

lead to an increase in irregular astigmatism and myopia, causing severe visual distortion. However, despite considerable effort, the exact pathogenesis of keratoconus remains unclear. Previously, MPM was used to perform an *ex vivo* large-area scan of the corneal button from a 23-year-old woman with bilateral keratoconus that underwent penetrating keratoplasty.[64] A comparison between the multiphoton and topographic images shown in Fig. 6 revealed that the AF mass composed of epithelial cells is consistent in position with the margin of the cone area and the keratoconic apex shown in the topographic map. Multiphoton imaging also reveals the presence of AF epithelial cells in Areas I and IV. In addition, collagen fibers were aligned and surround the proposed apical domain (white arrow). The enlarged images in Fig. 7 show that both the AF epithelial cells and collagen fiber orientation can be characterized. As shown in Figs. 7 I and I-1, AF epithelial cells were elongated and spindle-like in shape. In addition, Figs. 7 III and 7 III-1 illustrated the reorganization of the collagen fibers into thick and elongated bundles surrounding the proposed apical domain. These results show that MAF and SHG microscopy can effectively image the epithelial cells and collagen lamella structural alteration due to keratoconus. It also indicates that MPM may provide important morphological information of the investigation of the pathogenesis of keratoconus and may have potential in a clinical

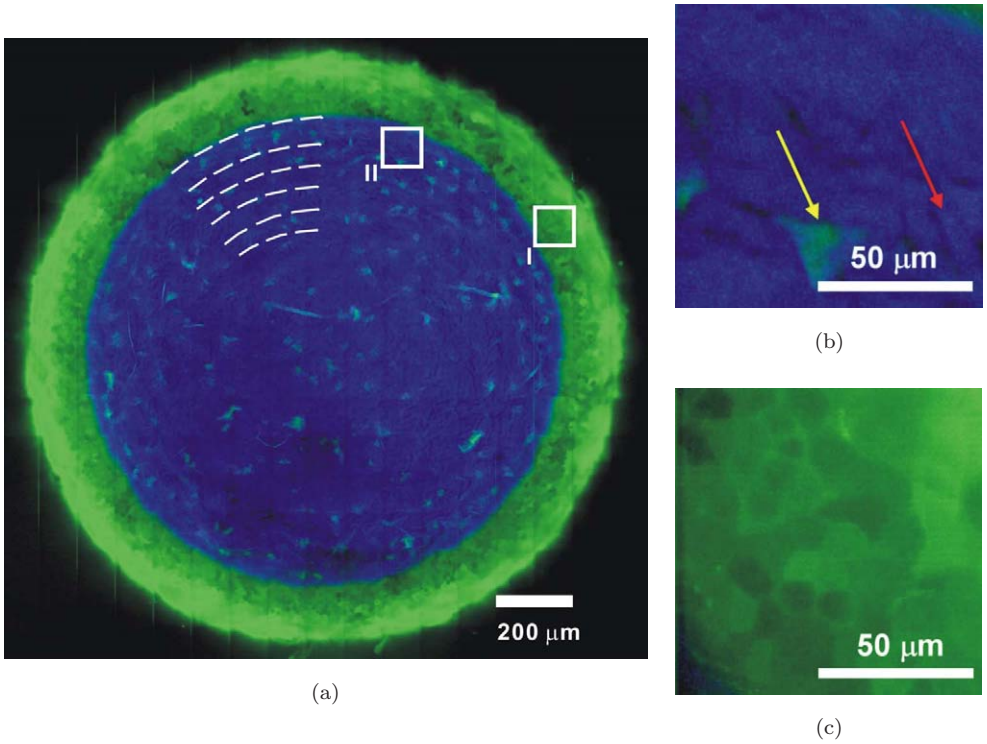

(a) (b) (c)

Fig. 5. (a) A multiphoton image across the entire cornea of a GFP mouse. Due to the nature curvature of cornea, the periphery of the circular cornea image indicates the superficial epithelium while the central area represents the depth of 300 μm, the approximate corneal thickness at the center of mouse cornea. (b) The magnified image of area II. Fluorescence from keratocytes (yellow arrow) and SHG from collagen (red arrow) can be observed. (c) The magnified image of area I within the epithelium. Reproduced with permission.

setting as an *in vivo* diagnostic and monitoring system for advancing keratoconus.

3.2.2. *Acanthamoeba castellinii keratitis coinfected with Pseudomonas aeruginosa*

Infection keratitis is one of the major causes responsible for visual loss and is of great significance in clinical practice. Timely diagnosis and application of anti-microbial treatment are important for treating this disease. Currently, clinical diagnosis relies mainly on examinination of the cultures of corneal scraping and biopsies. However, cultures and biopsies may not provide the correct diagnosis for appropriate anti-microbial treatment in time, and some recalcitrant infectious keratitis may be difficult to be differentiated according to existing clinical protocols.[65,66] Therefore, an imaging technique that can provide an early identification of the pathogens is of great value for the clinical diagnosis of infected corneas. The ability of *ex vivo* MPM in diagnosing infectious keratitis was demonstrated in the corneal specimen from a 12-year-old male who was diagnosed to have the co-infection of *A. castellinii* and *P. aeruginosa*.[67] In the large-scaled image (Fig. 8(a)), autofluorescent *Acanthamoeba* cysts (yellow arrows) as well as autofluorescent *bacilli* (red arrow) can be identified within the infected corneal stroma. In the magnified images of the selected areas in Fig. 8(a), individual spots can be visualized with intrinsic fluorescence (Fig. 8(b), red arrows) along with autofluorescent *Acanthamoeba* cysts (Figs. 8(b) and 8(c), yellow arrow). Comparison with the multiphoton image of isolated *P. aeruginosa* (Fig. 8(e)) suggest that the autofluorescent spots represented in Fig. 8(b) are mostly likely the individual bacteria. While second harmonic generating signal from collagen can still be observed (Fig. 8(d), blue), the observed structure lacked the regular collagen organization found in the less-infected stroma. In addition, the observed *Acanthamoeba* cysts within areas with relatively undestroyed collagen structure and minimal infiltration of inflammatory cells (Fig. 8(d), yellow arrow) implicate the possible residence of quiescent *Acanthamoeba* cysts within the clinically clear area. This observation may be helpful for the design of

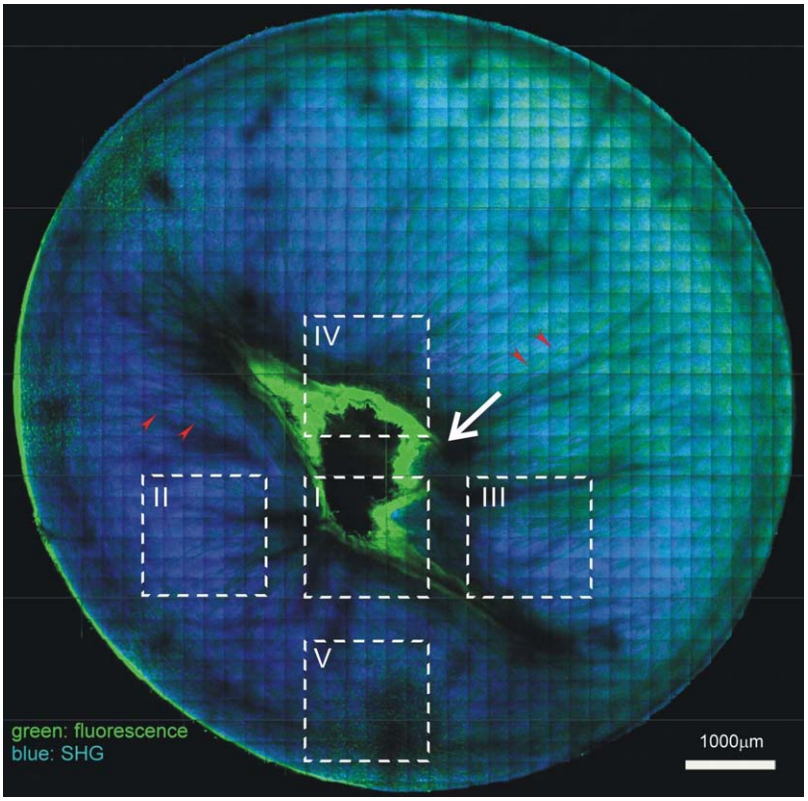

(a)

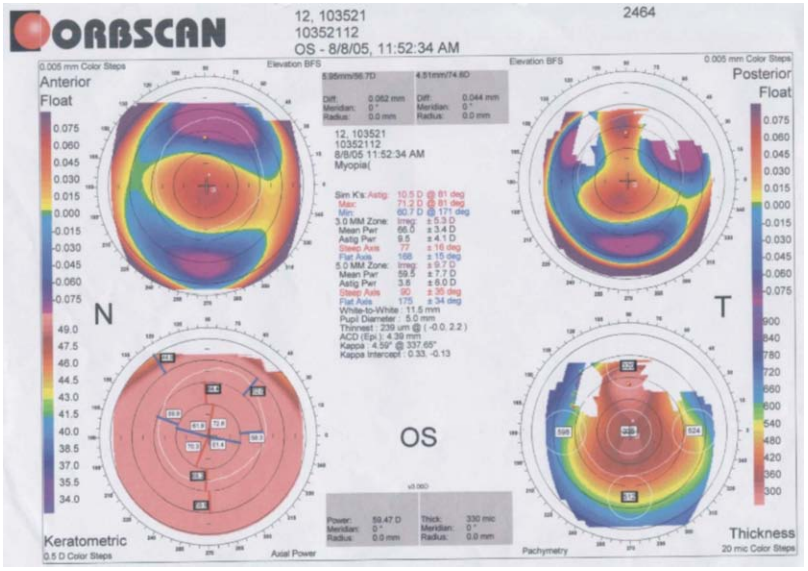

(b)

Fig. 6. A 33-year-old woman with bilateral keratoconus underwent penetrating keratoplasty in the left eye, due to the failure of visual correction by wearing rigid contact lens. (a) The multiphoton cross-sectional imaging of the entire corneal button (7.5 mm in diameter). Autofluorescent clusters are presented in the paracentral area, with SHG collagen fibers surrounding the apical domain (arrowheads). (b) The paracentral autofluorescent cluster (arrow) correlates with the apical area. (*Green*: MAF, *blue*: SHG). Reproduced with permission.

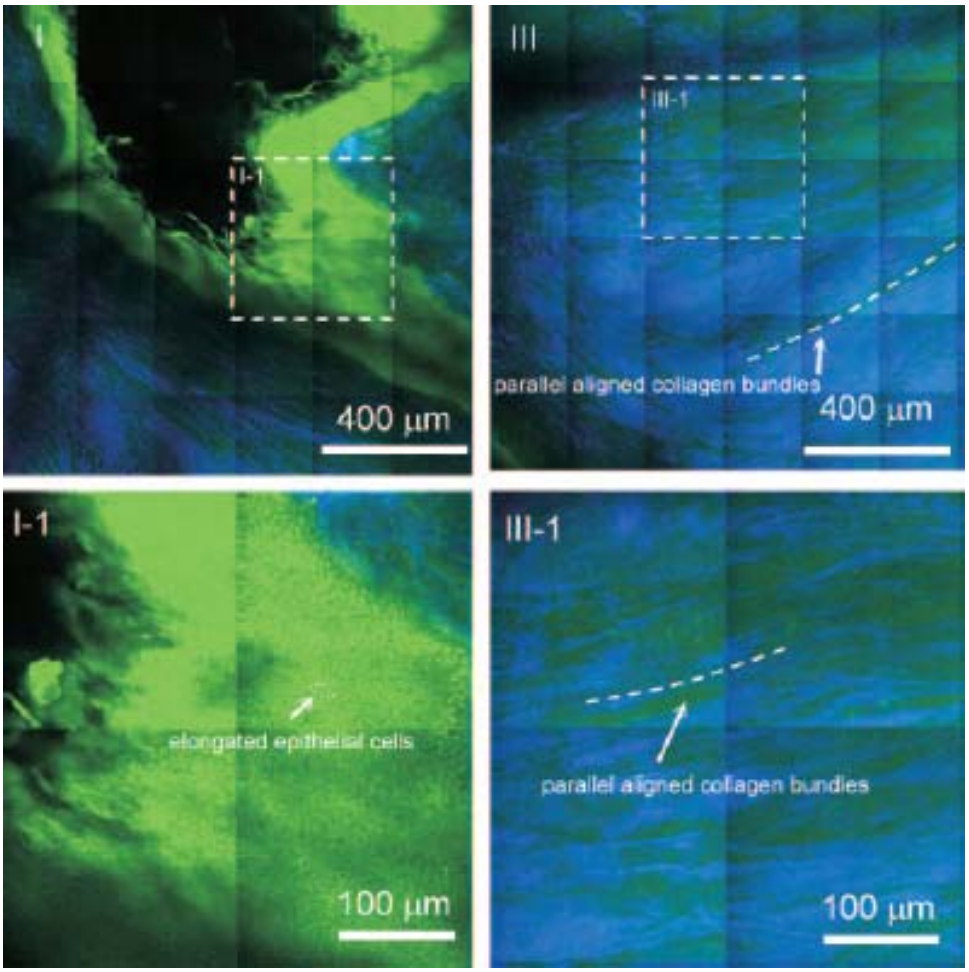

Fig. 7. Multiphoton images acquired from areas I and III in Fig. 6 are further analyzed. In area I, elongated fluorescent epithelial cells are identifiable. In area III, parallel-aligned pattern of SHG signals is seen. Magnified images of selected areas within areas I and III are shown (I-1 and III-1). (*Green*: MAF, *blue*: SHG). Reproduced with permission.

treatment strategy at the late stage of infection, and demonstrates that multiphoton imaging could provide morphological information of the extent of collagen destruction, inflammatory cell infiltration, and pathogen identification in infectious keratitis.

3.3. *Corneal scar tissue in penetrating full-thickness wound*

Another pathological condition that can be diagnosed by MPM is corneal scar. Any pathological abnormality from the wound healing processes and the associated disruption of collagen alignment may hinder cornea transparency and result in vision loss. Therefore, understanding wound healing process is important, especially in relevance to clinical refractive surgical. An example is shown in the multiphoton image of a corneal scar specimen from a 52-year-old man's right eye that received penetrating keratoplasty 10 years following trauma.[68] A number of pathological and physiological features can be identified in Fig. 9. First, the image at the depth of 0 μm shows the disruption of the Bowman's membrane with protruding SHG stromal collagen. At this depth, one can easily visualize fluorescent epithelial cells of the normal cornea. At the imaging depths of 1200 μm, an intense fluorescence lining (possibly from detached uveal tissue) along the wound edge is found. In addition, the collagen fibers outside of the wound tended to align parallel to the wound edges. These results illustrate that MPM can be used to identify structural alteration of a full-thickness linear corneal scar without histological procedures, and can potentially lead to a better understanding of the corneal wound healing process.

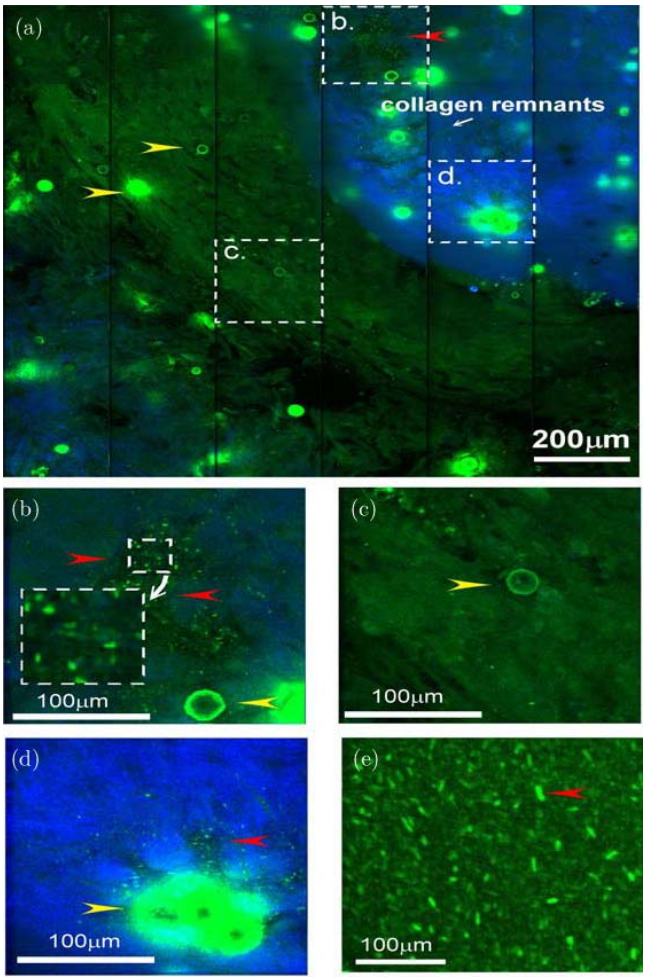

Fig. 8. (a) The large-area multiphoton image of *A. keratitis* coinfected with *P. aeruginosa*. Three selected regions in: (a) are magnified in (b), (c), and (d). The multiphoton image of *P. aeruginosa* colony is shown in (e). The red arrows in these images indicate the co-infected *P. aeruginosa* while all yellow arrows indicate *Acanthamoeba* cysts. (*Green*: MAF, *blue*: SHG). Reproduced with permission.

3.4. *Corneal wound healing — conductive keratoplasty (CK)*

In refractive surgical procedures, techniques based on different physical mechanism have proven to be effective in vision improvement. Conductive keratoplasty (CK) is a commonly applied surgical procedure for presbyopia and hyperopia correction, where corneal collagen is shrunk using thermal treatment.[69−72] Since such a refractive surgical procedure involves corneal remodeling, the mechanical investigation of the post-surgical regression process is important for the improvement in CK procedure and providing care for patients. Currently, conventional histopathological examination is still the primary tool for the evaluation of the corneal wound healing after refractive surgery. However, it has limited capacity for investigating the architecture of collagen fiber, the key element of wound healing after refractive surgery, and for studying the dynamical processes of corneal stroma. In a previously published report, the feasibility of using multiphoton imaging for characterizing the extent of *ex vivo*, post-CK corneal structural alteration was demonstrated.[73] In that work, CK was performed on the right eyes of New Zealand albino rabbits at the setting of about 0.3 W for 0.6 seconds while the left eyes were punctured by keratoplast tip without the application of thermal energy (control group). The MAF and SHG images of the *ex vivo* rabbit cornea scanned along different depths were obtained at four time points — Day 1 and Weeks 1, 2, and 4 — following the CK procedure (Fig. 10). All the images were oriented in the same fashion with the epithelium side up. In all images, the CK sites (red arrows) can be characterized by the absence of SHG. In the Day 1 images, epithelial injuries were observed in both the CK and control corneas, due to insertion of the keratoplast tip. Re-epithelialization of both the CK and control groups is accomplished within one week. However, compensatory epithelial hyperplasia is observed at the wounding site of CK corneas. The hyperplasia persisted for at least 4 weeks after the CK procedure. Comparing the mechanical wound in the control cornea, induced collagen damage in CK cornea resulted in a larger area with no SHG signal. Therefore, MAF and SHG imaging can be utilized for *ex vivo* observation of structural alterations and for the subsequent wound healing of cornea from CK.

3.5. *Quantitative analysis of corneal thermal denaturation by SHG microscopy*

Thermal effects on corneal collagen are of great concern in corneal physiology as therapeutic procedures and refractive surgeries may be based on the application of heat. However, there are still few effective imaging techniques providing immediate and quantitative information characterization of the thermal denaturation of corneal collagen. However, as demonstrated earlier, SHG microscopy may be used to qualitatively and quantitatively characterize thermal damage to porcine cornea in intact porcine eyes *ex vivo*.[74] Quantitative analysis of the thermal effect on cornea collagen was

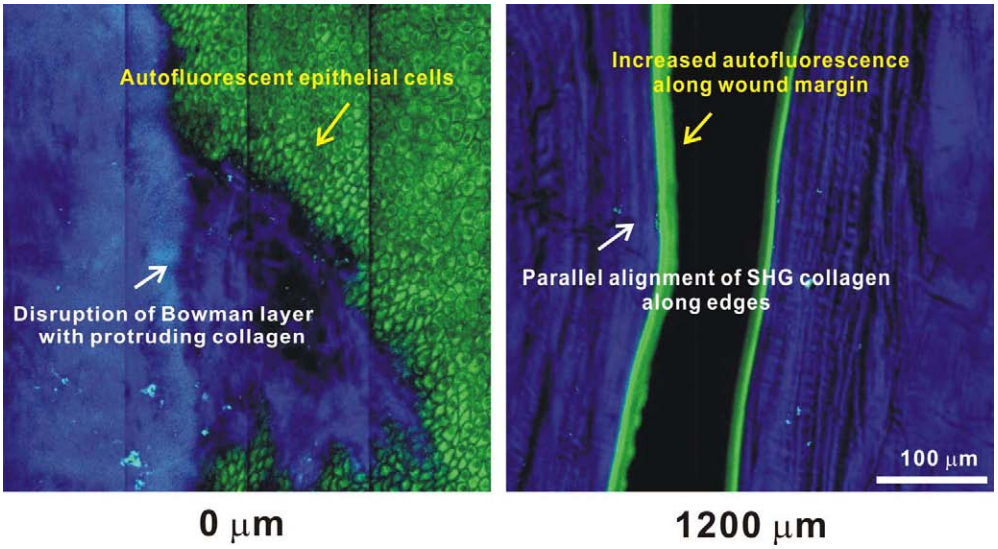

Fig. 9. *Ex vivo* multiphoton images of the penetrating corneal scar tissue. Three-dimensional projected images at 0 and 1200 μm. (*Green*: MAF, *blue*: SHG). Reproduced with permission.

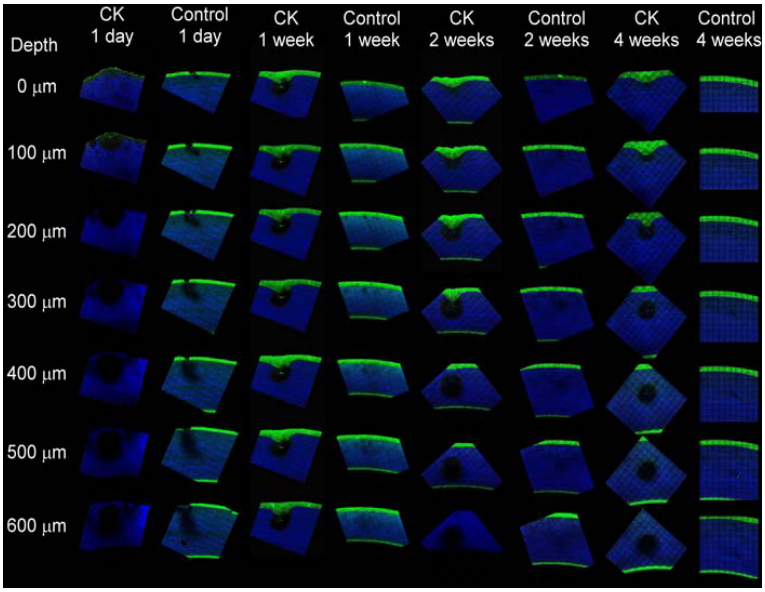

Fig. 10. The depth-dependent multiphoton corneal images are obtained after different time points following CK and control treatments. (*Green*: MAF, *blue*: SHG). Reproduced with permission.

performed by averaging the SHG intensity across the large-area scan of porcine eyeballs that were placed in a heated buffer bath with different temperatures for 5 minutes.[75] For each temperature, the results of the SHG intensity from three sets of porcine corneas were averaged and plotted (Fig. 11). The SHG signals were observed to peak at 53°C, 65°C, and 74°C to 77°C, possibly due to the organization of collagen fibers into locally dense structures during the thermal treatment process. The sharp rise at 65°C can be attributed to a sharp, irreversible structural change of the cornea stroma at that temperature. The lack of SHG signal at 90°C suggests that at sufficiently high temperatures, neither the cross-linking nor the hydrogen bonds within corneal stroma has the strength to maintain the structure of collagen fibers responsible for generating the SHG signal. Therefore, the nonlinear imaging modality of SHG microscopy may be used to obtain qualitative and quantitative information of collagen structural alteration in thermally treated corneas.

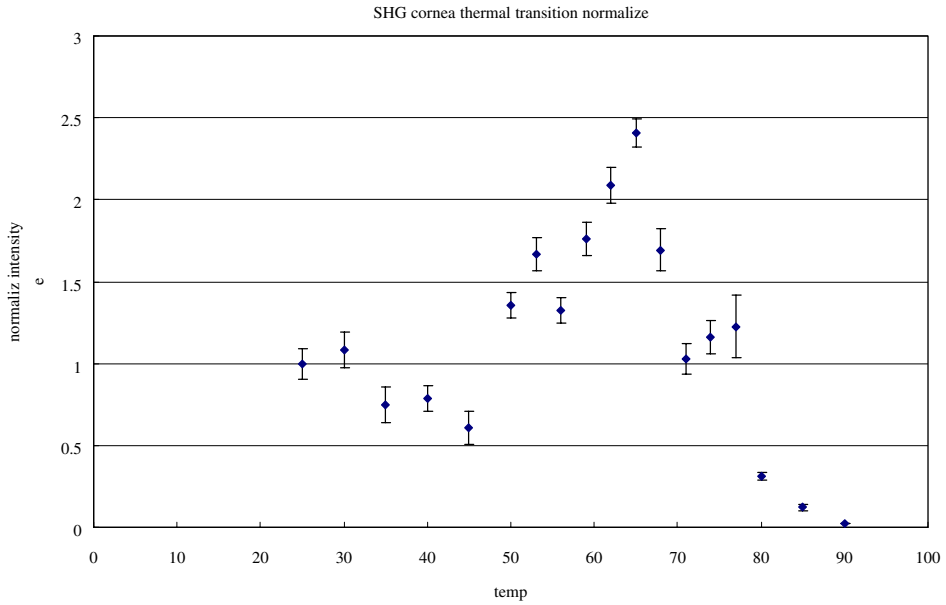

Fig. 11. Second harmonic intensity of porcine cornea stroma as a function of treatment temperature. All corneas were treated for 5 minutes. Reproduced with permission.

4. Conclusion

The minimal invasion and the ability to resolve corneal structures over the whole cornea renders MPM a potential technique for *in vivo* corneal imaging modality with potential clinical applications. However, prior to performing *in vivo* and clinical studies, *ex vivo* examination with this imaging technique needs to be established. In this review article, we demonstrated a series of *ex vivo* morphological investigation on cornea physiology, pathology, wound healing, and corneal thermal denaturation by the use of MAF and SHG microscopy. Using this approach, cellular component and collagen fibers within the whole cornea and ocular surface can be imaged at sub-micron resolution. In addition, corneal structural alteration due to the pathological conditions of keratoconus and infected keratitis can be observed with MPM. These results also reveal that MPM may be effective for real-time detection of pathogens and for identification of different pathogens. Furthermore, multiphoton investigation of corneal scar and structural alteration following CK has provided additional insights into the mechanics of the corneal wound healing process. With additional development, MPM can become an effective imaging technique for the *in vivo* investigation of corneal physiological processes and clinical diagnosis of corneal diseases.

Acknowledgment

We would like to acknowledge the support of the National Research Program of Genomic Medicine (NRPGM) of the National Science Council (NSC) in Taiwan. This work was completed in the Optical Molecular Imaging Microscopy Core Facility (A5) of NRPGM.

References

1. Crown, L. A., "Introduction to slit lamp biomicroscopy," *Am. J. Clin. Med.* **3**, 12 (2006).
2. Gullstrand, A., "Demonstration der Nernstspaltlampe," *Presentacion al congreso de la Sociedad Alemana de Oftalmologia. Heidelberg* (1911).
3. Martin, C. L., "Slit lamp examination of the normal Canine anterior ocular segment: Part I-Introduction and Technique*," *J. Small Ani. Pract.* **10**, 143–149 (1969).
4. Mishima, S., Gasset, A., Klyce, S. D. and Baum, J. L., "Determination of tear volume and tear flow," *Invest. Ophth. Vis. Sci.* **5**, 264–276 (1966).
5. Waltman, S. R. and Kaufman, H. E., "A new objective slit lamp fluorophotometer," *Invest. Ophth. Vis. Sci.* **9**, 247–249 (1970).
6. Hirano, K., Ito, Y., Suzuki, T., Kojima, T., Kachi, S. and Miyake, Y., "Optical coherence tomography for the noninvasive evaluation of the cornea," *Cornea* **20**, 281 (2001).
7. Huang, D., Swanson, E. A., Lin, C. P., Schuman, J. S., Stinson, W. G., Chang, W., Hee, M. R.,

Flotte, T., Gregory, K. and Puliafito, C. A., "Optical coherence tomography," *Science* **254**, 1178–1181 (1991).
8. Fukuchi, T., Takahashi, K., Shou, K. and Matsumura, M., "Optical coherence tomographic (OCT) findings on normal retina and laser induced choroidal neovascularisation (CNV) in rat," *Invest. Ophth. Vis. Sci.* **41**, S174–S174 (March 15, 2000).
9. Fujimoto, J. G., "Optical coherence tomography for ultrahigh resolution *in vivo* imaging," *Nat. Biotechnol.* **21**, 1361–1367 (November 2003).
10. Brezinski, M. E. and Fujimoto, J. G., "Optical coherence tomography: high-resolution imaging innontransparent tissue," *Sel. Top. Quantum Electron. IEEE J.* **5**, 1185–1192 (1999).
11. Swanson, E. A., Izatt, J. A., Hee, M. R., Huang, D., Lin, C. P., Schuman, J. S., Puliafito, C. A. and Fujimoto, J. G., "*In vivo* retinal imaging by optical coherence tomography," *Opt. Let.* **18**, 1993–1911 (1993).
12. Izatt, J. A., Hee, M. R., Swanson, E. A., Lin, C. P., Huang, D., Schuman, J. S., Puliafito, C. A. and Fujimoto, J. G., "Micrometer-scale resolution imaging of the anterior eye *in vivo* with optical coherence tomography," *Arch. Ophthalmol.* **112**, 1584–1589 (1994).
13. Hoerauf, H., Wirbelauer, C., Scholz, C., Engelhardt, R., Koch, P., Laqua, H. and Birngruber, R., "Slit-lamp-adapted optical coherence tomography of the anterior segment," *Graef. Arch. Clinic. Exp. Ophthalmol.* **238**, 8–18 (2000).
14. Wang, J., Simpson, T. L. and Fonn, D., "Objective measurements of corneal light-backscatter during corneal swelling, by optical coherence tomography," *Invest. Ophth. Vis. Sci.* **45**, 3493 (2004).
15. Puliafito, C. A., Hee, M. R., Lin, C. P., Reichel, E. J., Schuman, S. J., Duker, S., Izatt, J. A., Swanson, E. A. and Fujimoto, J. G., "Imaging of macular diseases with optical coherence tomography," *Ophthalmology* **102**, 217–29 (1995).
16. Minsky, M., "Memoir on inventing the confocal scanning microscope," *Scanning* **10**, 128–138 (July–August 1988).
17. Petran, M., Hadravsky, M., Egger, M. D. and Galambos, R., "Tandem-scanning reflected-light microscope," *J. Opt. Soc. Am.* **58**, 90–93 (1968).
18. Egger, M. D., "Observation of nerve fibers in incident light," *Experientia (Basel)* **25**, 1225 (1969).
19. Bohnke, M. and Masters, B. R., "Confocal microscopy of the cornea," *Prog. Retin. Eye Res.* **18**, 553–628 (1999).
20. Masters B. R. and Bohnke, M., "Three-dimensional confocal microscopy of the human cornea *in vivo*," *Ophthal. Res.* **33**, 125–135 (May–June 2001).
21. Masters B. R. and Bohnke, M., "Three-dimensional confocal microscopy of the living human eye," *Annu. Rev. Biomed. Eng.* **4**, 69–91 (2002).
22. Chen, W. L., Chang, H. W. and Hu, F. R., "*In vivo* confocal microscopic evaluation of corneal wound healing after epi-LASIK," *Invest. Ophth. Vis. Sci.* **49**, 2416–2423 (June 2008).
23. Moller-Pedersen, T., Cavanagh, H. D., Petroll, W. M. and Jester, J. V., "Mechanisms of regression and haze development after excimer laser PRK — A one-year confocal microscopic study," *Invest. Ophth. Vis. Sci.* **40**, S108–S108 (March 15, 1999).
24. Moller-Pedersen, T., Cavanagh, H. D., Petroll, W. M. and Jester, J. V., "Stromal wound healing explains refractive instability and haze development after photorefractive keratectomy — A one-year confocal microscopic study," *Ophthalmology* **107**, 1235–1245 (July 2000).
25. Moller-Pedersen, T. H., Li, F., Petroll, W. M., Cavanagh, H. D. and Jester, J. V., "Confocal microscopic characterization of wound repair after photorefractive keratectomy," *Invest. Ophth. Vis. Sci.* **39**, 487–501 (March 1998).
26. Chen, W. L., Sun, Y., Lo, W., Tan, H. Y. and Dong, C. Y., "Combination of multiphoton and reflective confocal imaging of cornea," *Microsc. Res. Tech.* **71**, 83–85 (February 2008).
27. Hollingsworth, J. G., Bonshek, R. E. and Efron, N., "Correlation of the appearance of the keratoconic cornea *in vivo* by confocal microscopy and in vitro by light microscopy," *Cornea* **24**, 397–405 (May 2005).
28. Linna, T. and Tervo, T., "Real-time confocal microscopic observations on human corneal nerves and wound healing after excimer laser photorefractive keratectomy," *Curr. Eye Res.* **16**, 640–649 (July 1997).
29. MollerPedersen, T., Vogel, M., Li, H. F., Petroll, W. M., Cavanagh, H. D. and Jester, J. V., "Quantification of stromal thinning, epithelial thickness, and corneal haze after photorefractive keratectomy using *in vivo* confocal microscopy," *Ophthalmology* **104**, 360–368 (March 1997).
30. Jalbert, I., Stapleton, F., Papas, E., Sweeney, D. F. and Coroneo, M., "*In vivo* confocal microscopy of the human cornea," *Brit. Med. J.* **87**, 225–236 (2003).
31. Patel, S. V., McLaren, J. W., Hodge, D. O. and Bourne, W. M., "Normal human keratocyte density and corneal thickness measurement by using confocal microscopy *In Vivo*," *Invest. Ophth. Vis. Sci.* **42**, 333–339 (2001).
32. Hollingsworth, J. G., Bonshek, R. E. and Efron, N., "Correlation of the appearance of the Keratoconic cornea *In Vivo* by confocal microscopy and in vitro by light microscopy," *Cornea* **24**, 397 (2005).
33. Cavanagh, H. D., Petroll, W. M., Alizadeh, H., He, Y. U. G., McCulley, J. P. and Jester, J. V., "Clinical and diagnostic use of *in vivo* confocal microscopy

in patients with corneal disease," *Ophthalmology (Rochester, MN)* **100**, 1444–1454 (1993).
34. Beuerman, R. W., Chew, S. J., Pedroza, L., Assouline, M., Barron, B., Hill, J. and Kaufman, H. E., "Early diagnosis of infectious Keratitis with *In vivo* real-time confocal microscopy," *Invest. Ophth. Vis. Sci.* **33**, 1234–1234, (March 15 1992).
35. Pfister, D. R., Cameron, J. D., Krachmer, J. H. and Holland, E. J., "Confocal microscopy findings of Acanthamoeba keratitis," *Am. J. Ophth.* **121**, 119–128 (February 1996).
36. Nakano, E., Oliveira, M., Portellinha, W., de Freitas, D. and Nakano, K., "Confocal microscopy in early diagnosis of Acanthamoeba keratitis," *J. Refract. Surg.* **20**, S737–S740 (September–October 2004).
37. Balestrazzi, A., Martone, G., Traversi, C., Haka, G., Toti, P. and Caporossi, A., "Keratoconus associated with corneal macular dystrophy: *In vivo* confocal microscopic evaluation," *Euro. J. Ophthalmol.* **16**, 745–750 (September–October 2006).
38. Mazzotta, C., Baiocchi, S., Caporossi, O., Buccoliero, D., Casprini, F., Caporossi, A. and Balestrazzi, A., "Confocal microscopy identification of keratoconus associated with posterior polymorphous corneal dystrophy," *J. Cataract Refr. Surg.* **34**, 318–321 (February 2008).
39. Denk, W., Strickler, J. H. and Webb, W. W., "2-Photon laser scanning fluorescence microscopy," *Science* **248**, 73–76 (April 6 1990).
40. So, P. T. C., Dong, C. Y., Masters, B. R. and Berland, K. M., "Two-P hoton excitation fluorescence microscopy," *Annu. Rev. Biomed. Eng.* **2**, 399–429 (2000).
41. Chen, W. L., Lo, W., Sun, Y., Lin, S. J., Tan, H. Y. and Dong, C. Y., "The combination of multiphoton and reflected confocal microscopy for cornea imaging," *Proc. SPIE* **6138**, 61380M (2006).
42. Masters, B. R., Piston, D. W. and Webb, W. W., "3-dimensional Nad(P)H redox imaging of the insitu cornea with 2 photon excitation laser scanning microscopy," *Invest. Ophth. Vis. Sci.* **34**, 1402–1402 (March 15 1993).
43. Piston, D. W., Masters, B. R. and Webb, W. W., "Three-dimensionally resolved NAD(P)H cellular metabolic redox imaging of the *in situ* cornea with two-photon excitation laser scanning microscopy," *J. Microsc.* **178**, 20–27 (1995).
44. Zipfel, W. R., Williams, R. M. and Webb, W. W., "Nonlinear magic: multiphoton microscopy in the biosciences," *Nat. Biotechnol.* **21**, 1368–1376 (November 2003).
45. Campagnola, P. J. and Loew, L. M., "Second-harmonic imaging microscopy for visualizing biomolecular arrays in cells, tissues and organisms," *Nat. Biotechnol.* **21**, 1356–1360 (2003).
46. Goppert-Mayer, M., "Elementary file with two quantum fissures," *Ann. Phys.* **9**, 273–294 (May 1931).
47. Kaiser, W. and Garrett, C. G. B., "2-photon excitation in Caf2 — Eu2+," *Phys. Rev. Lett.* **7**, 229 (1961).
48. Franken, P. A., Hill, A. E., Peters, C. W. and Weinreich, G., "Generation of optical harmonics," *Phys. Rev. Lett.* **7**, 118–119 (1961).
49. Gannaway, J. N., "Second-harmonic imaging in the scanning optical microscope," *Opt. Quant. Electron.* **10**, 435 (1978).
50. Helmchen, F., "Deep tissue two-photon microscopy," *Nat. Methods* **2**, 932 (2005).
51. Zipfel, W. R., Williams, R. M. and Webb, W. W., "Nonlinear magic: multiphoton microscopy in the biosciences," *Nat. Biotechnol.* **21**, 1369–1377 (2003).
52. Sun, C. K., Chu, S. W., Chen, S. Y., Tsai, T. H., Liu, T. M., Lin, C. Y. and Tsai, H. J. "Higher harmonic generation microscopy for developmental biology," *J. Struct. Biol.* **147**, 19–30 (2004).
53. Forrester, J. V., *The Eye: Basic Sciences in Practice*, 2nd Ed. (W. B. Saunders, Edinburgh; New York, 2002).
54. Fine, S., "Optical second harmonic generation in biological systems," *Scanning* **340**, 360 (1971).
55. Mertz, J. and Moreaux, L., "Second-harmonic generation by focused excitation of inhomogeneously distributed scatterers," *Opt. Communi.* **196**, 325–330 (2001).
56. Lyubovitsky, J. G., Spencer, J. A., Krasieva, T. B., Andersen, B. and Tromberg, B.J., "Imaging corneal pathology in a transgenic mouse model using nonlinear microscopy," *J. Biomed. Opt.* **11**, 014013 (2006).
57. Yeh, A. T., Nassif, N., Zoumi, A. and Tromberg, B. J., "Selective corneal imaging using combined second-harmonic generation and two-photon excited fluorescence," *Opt. Lett.* **27**, 2082–2084 (2002).
58. Morishige, N., Wahlert, A. J., Kenney, M. C., Brown, D. J., Kawamoto, K., Chikama, T., Nishida, T. and Jester, J. V., "Second-harmonic imaging microscopy of normal human and Keratoconus cornea," *Invest. Ophth. Vis. Sci.* **48**, 1087–1094 (2007).
59. Han, M., Giese, G. and Bille, J. F., "Second harmonic generation imaging of collagen fibrils in cornea and sclera," *Opt. Express* **13**, 5791–5797 (July 25, 2005).
60. Teng, S. W., Tan, H. Y., Peng, J. L., Lin, H. H., Kim, K. H., Lo, W., Sun, Y., Lin, W. C., Lin, S. J. and Jee, S. H., "Multiphoton autofluorescence and second-harmonic generation imaging of the *ex vivo* Porcine eye," *Invest. Ophth. Vis. Sci.* **47**, 1216–1224 (2006).

61. Lo, W. S., Teng, W. H., Tan, Y., Kim, K. H., Chen, H. C., Lee, H. S., Chen, Y. F., So, P. T. C. and Dong, C. Y., "Intact corneal stroma visualization of GFP mouse revealed by multiphoton imaging," *Microsc. Res. Tech* **69**, 973–975 (2006).
62. Ragan, T., Sylvan, J. D., Kim, K., Huang, H. H., Bahlmann, K., Lee, R. T. and So, P. T. C., "High-resolution whole organ imaging using two-photon tissue cytometry," *J. Biomed. Opt.* **12**, 014015 (2007).
63. Rabinowitz, Y. S., "Keratoconus," *Surv. Ophth.* **42**, 297–319 (January–February 1998).
64. Tan, H. Y., Sun, Y., Lo, W., Lin, S. J., Hsiao, C. H., Chen, Y. F.,. Huang, S. C. M, Lin, W. C., Jee, S. H. and Yu, H. S., "Multiphoton fluorescence and second harmonic generation imaging of the structural alterations in Keratoconus ex vivo," *Invest. Ophth. Vis. Sci.* **47**, 5251–5259 (2006).
65. Radford, C. F., Minassian, D. C. and Dart, J. K. G., "Acanthamoeba keratitis in England and Wales: incidence, outcome, and risk factors," *Brit. Med. J.* **86**, 536–542 (2002).
66. Bacon, A. S., Frazer, D. G., Dart, J. K., Matheson, M., Ficker, L. A. and Wright, P., "A review of 72 consecutive cases of Acanthamoeba keratitis, 1984–1992," *Eye* **7**, 719–25 (1993).
67. Tan, H. Y., Sun, Y., Lo, W., Teng, S. W., Wu, R. J., Jee, S. H., Lin, W. C., Hsiao, C. H., Lin, H. C. and Chen, Y. F., "Multiphoton fluorescence and second harmonic generation microscopy for imaging infectious keratitis," *J. Biomed. Opt.* **12**, 024013 (2007).
68. Teng, S. W., Tan, H. Y., Sun, Y., Lin, S. J., Lo, W., Hsueh, C. M., Hsiao, C. H., Lin, W. C., Huang, S. C. M. and Dong, C. Y., "Multiphoton fluorescence and second-harmonic-generation microscopy for imaging structural lterations in corneal scar tissue in penetrating full-thickness wound," *Arch. Ophth.* **125**, 977 (2007).
69. Haw W. W. and Manche, E. E., "Conductive keratoplasty and laser thermal keratoplasty," *Int. Ophthalmol. Clin.* **42**, 99–106 (Fall 2002).
70. Huang, B., "Update on nonexcimer laser refractive surgery technique: conductive keratoplasty," *Curr. Opin. Ophthalmol.* **14**, 203–206 (August 2003).
71. McDonald, M. B., Durrie, D., Asbell, P., Maloney, R. and Nichamin, L., "Treatment of presbyopia with conductive keratoplasty (R) — six-month results of the 1-year United States FDA clinical trial," *Cornea* **23**, 661–668 (October 2004).
72. McDonald, M. B., Hersh, P. S., Manche, E. E., Maloney, R. K., Davidorf, J. and Sabry, M., "Conductive keratoplasty for the correction of low to moderate hyperopia: US clinical trial 1-year results on 355 eyes," *Ophthalmology* **109**, 1978–1989 (November 2002).
73. Wang, T. J., Lo, W., Hsueh, C. M., Hsieh, M. S., Dong, C. Y. and Hu, F. R., "Ex vivo multiphoton analysis of rabbit corneal wound healing following conductive keratoplasty," *J. Biomed. Opt.* **13**, 034019 (May–Jun 2008).
74. Tan, H. Y., Teng, S. W., Lo, W., Lin, W. C., Lin, S. J., Jee, S. H. and Dong, C. Y., "Characterizing the thermally induced structural changes to intact porcine eye, Part 1: second harmonic generation imaging of cornea stroma," *J. Biomed. Opt.* **10**, 054019 (2005).
75. Kampmeier, J., Radt, B., Birngruber, R. and Brinkmann, R., "Thermal and biomechanical parameters of porcine cornea," *Cornea* **19**, 355 (2000).